Tech Science Press

Locating Famous Tea's Picking Point Based on Shi-Tomasi Algorithm

Lei Zhang[1,2], Lang Zou[1,2], Chuanyu Wu[1,2,*], Jianneng Chen[1,2] and Heping Chen[3]

[1]Faculty of Mechanical Engineering & Automation, Zhejiang Sci-Tech University, Hangzhou, 310018, China
[2]Key Laboratory of Transplanting Equipment and Technology of Zhejiang Province, Hangzhou, 310018, China
[3]Ingram School of Engineering, Texas State University, San Marcos, Texas, USA
[*]Corresponding Author: Chuanyu Wu. Email: cywu@zstu.edu.cn

Abstract: To address the difficulty of locating the picking point of a tea sprout during the intelligent automatic picking of famous tea, this study proposes a method to obtain information on the picking point on the basis of the *Shi-Tomasi* algorithm. This method can rapidly identify a tea sprout's picking point and obtain its coordinates. Images of tea sprouts in a tea garden were collected, and the G-B component of tea sprouts was segmented using the Otsu algorithm. The region of interest was set with the lowest point of its contour as the center. The characteristics of tea buds and branches in the area were extracted, and the Otsu algorithm was used for a second segmentation of tea sprout images. The tea buds were segmented using the improved *Zhang* algorithm. The branch feature binary image was used to refine the skeleton, and the *Shi-Tomasi* algorithm was used to detect the corners of the skeleton and calculate and mark the picking points of the shoots. Sixty sets of samples were tested. The test identified 1,042 effective shoots for tender buds, and 887 picking points were marked, with a success rate of 85.12%, thereby verifying the effectiveness of the method and providing a theoretical reference for the visual positioning of the automatic picking of famous tea.

Keywords: Famous tea; picking location; Zhang algorithm; *Shi-Tomasi* algorithm

1 Introduction

The automatic recognition and positioning of picking points is a key technology enabling modern agricultural robots to achieve automatic and precise picking. Scholars have conducted considerable research on this topic because of the wide application of intelligent picking robots and the development of artificial intelligence recognition [1–5]. Liang et al. [6] calculated the position information of the picking point of tomato fruit bunch stems on the basis of the corner points of the stem skeleton, achieving a success rate of 90%. Yang et al. [7] constructed a recognition and positioning system based on a convolutional neural network and Kinect V2 for a citrus-picking robot. Huang et al. [8] realized the accurate positioning of objects on the basis of SSD detection and built the Kinect V2 three-dimensional measurement model. Xiong et al. [9] used Hough line fitting and the angle constraint method to realize the positioning of disturbed

grape picking points, obtaining an accuracy rate of 80%. Wang et al. [10] proposed an apple target picking point location method based on the contour symmetry axis. Luo et al. [11] proposed a grape picking point location method based on improved clustering image segmentation and a minimum distance constraint between points and lines.

"Famous tea" is a general term for high-quality tea, with strict requirements on the growth environment, picking time, picking method, and picking quality of the tea itself. The high-efficiency and high-quality picking of famous tea is desired. Vision-based automatic picking robots have come into use for picking famous teas. The automatic identification and positioning of picking points is a difficulty that limits the development of these robots. Few studies have been conducted on the positioning of famous tea picking points. Zhang et al. [12] proposed a tender shoot positioning method based on active vision. Pei et al. [13] marked the center of the circumscribed rectangle of the tea outline as the picking point.

Famous tea is lightweight; hence it swings easily because of wind or the movement of a picking machine. A tea garden has a complex environment, with tea leaves blocking each other. Light can be too strong or dark, resulting in low-resolution images of tea sprouts and old leaves. Therefore, it is difficult to identify and locate the shoot picking points, which restricts automated picking. To realize the rapid identification and positioning of picking points, ensure the efficiency of picking machines, and meet high quality requirements, this study proposes an automatic identification method for famous tea picking points based on the *Shi-Tomasi* algorithm.

2 Recognition Algorithm Based on Shi-Tomasi

Fig. 1 shows the algorithm's flowchart. The original image of tea growth and distribution is collected by an industrial camera. Image preprocessing is performed for raw image noise reduction, and the Otsu algorithm is used to segment the images to obtain a contour map of the tea sprouts. The lowest point of each contour is searched, the region of interest (ROI) of a single sprout is set, and the characteristics of sprouts and their growth branches are extracted. A second image segmentation and morphological processing are performed on these characteristics. The Otsu algorithm is used to binarize the image, and a morphological method is used to remove the noise of the binary image in post-processing. The skeleton of the sprouts and branches is refined using the improved Zhang thinning algorithm, and the *Shi-Tomasi* algorithm is used to extract the corner point at a bifurcation and obtain their coordinates. A line segment is fitted between the corner point and the lowest point. The center point's coordinates are calculated as the coordinates of picking points, which are marked in the original image.

3 Target Recognition of Tea Sprouts

3.1 Image Segmentation of Tea Sprouts

The initial segmentation of the tea sprouts is the basis for the accurate positioning of the picking points. We use the Otsu algorithm to perform the initial segmentation of the tea sprouts under the RGB model, and a 3×3 convolution kernel for Gaussian filtering of the collected tea image noise. For the tea sprouts shown in Fig. 2a, the differentiation degree between old leaves and tea sprouts is most obvious among the G-B components of the image in Fig. 2b. Thus the G-B component is used as the input source for image segmentation. The segmentation effect is shown in Fig. 2c. Some small, wrong target points or contours still exist because of noise and for other reasons. Morphological procedures facilitate later operations. The result is shown in Fig. 2d. The small contours caused by noise and other factors have been filtered out.
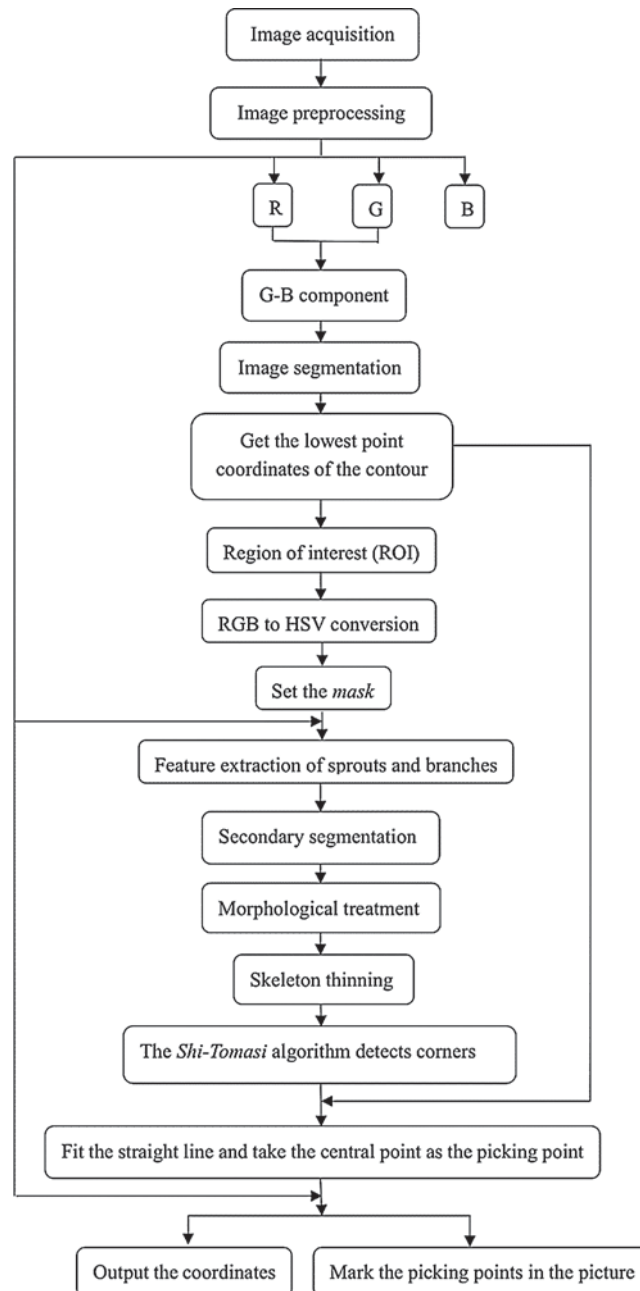
Figure 1: Flowchart of recognition algorithm based on *Shi-Tomasi*

3.2 Setting the ROI of Tea Sprouts

To reduce the influence of factors irrelevant to the picking point, and to reduce the number of pixels and improve the real-time performance of image processing, each sprout in image acquisition has its own ROI. Only this region is regarded as the target when identifying the picking point object. Based on research and experiments, the following search algorithm for setting the ROI with the lowest point of the contour of tea sprouts as the center is proposed.

(1) The edge points of each contour, as shown in Fig. 2c, are traversed. The lowest and highest points of contours are found, with coordinates set as (x_0, y_0) and (x_1, y_1), respectively.

(2) The contour height filter parameters are set to filter out some sprouts that are too small in the visible area because of occlusion and for other reasons. When the straight line between the highest and lowest points has length greater than or equal to a preset value D, the contour number i is entered in the list to be processed, $list[\ ]$; otherwise, it is discarded and recorded as $\varnothing$, as follows:

$$list[] = \left\{ \begin{array}{l} i, \sqrt{(y_1 - y_0)^2 + (x_1 - x_0)^2} \geq D \\ \varnothing, \sqrt{(y_1 - y_0)^2 + (x_1 - x_0)^2} < D \end{array} \right\}. \tag{1}$$

(3) With the lowest point $(x_0, \ y_0)$ of each contour in $list[\ ]$ as the center, a rectangular ROI is set with length Roi_L and height Roi_H,

$$\left\{ \begin{array}{l} Roi\_L = x_{max} - x_{min} \\ Roi\_H = y_{max} - y_{min} \end{array} \right\}, \tag{2}$$

where x_{min}, y_{max} and x_{max}, y_{min} are the coordinates of the top-left and bottom-right vertices, respectively, of the rectangular ROI. In this study, $x_{min} = x_0 - 30\ pixels$, $x_{max} = x_0 + 30\ pixels$, $y_{min} = y_0 - 30\ pixels$, and $y_{max} = y_0 + 25\ pixels$.

The ROI setting result is shown in Fig. 3. The red point is the lowest point of the contour of the sprout for first-time segmentation. Some points deviate from the actual picking point.
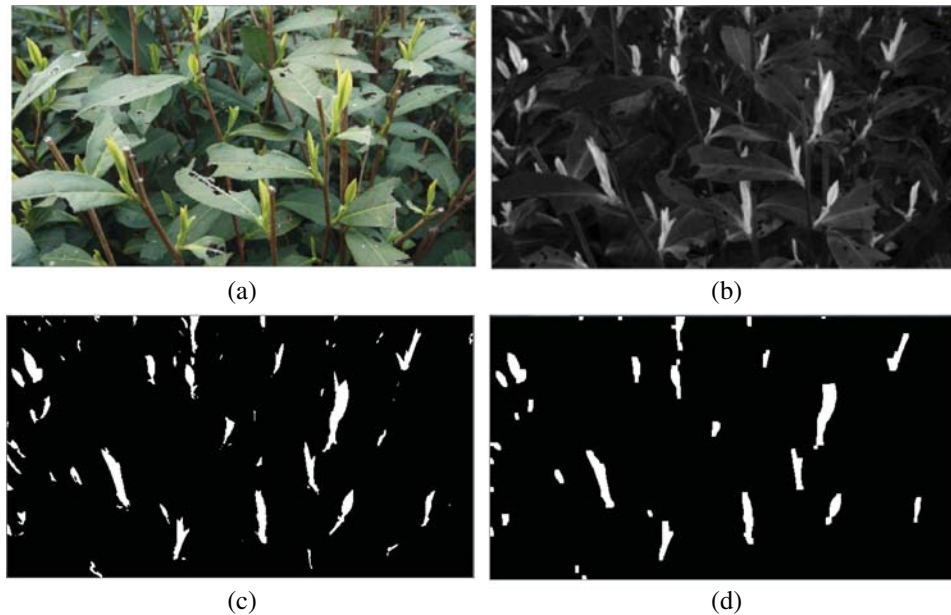

Figure 2: Image segmentation process. a. Original image b. G-B component c. Image segmentation d. Morphological operation

Figure 3: ROI

4 Picking Point Identification and Positioning

The quality requirements of famous tea make it necessary to ensure the integrity of sprouts and to limit the extraction of the petiole during picking. The growth characteristics of the tea suggest that its sprouts grow diagonally upward. The tea picking point calculation model is shown in Fig. 4. The growth point area of the sprouts on the branches is extracted to obtain the corner point position and picking point direction, and a straight line fits the corner point and lowest point. The coordinates of the picking point in the ideal area are calculated through a process combined with agronomic technology.
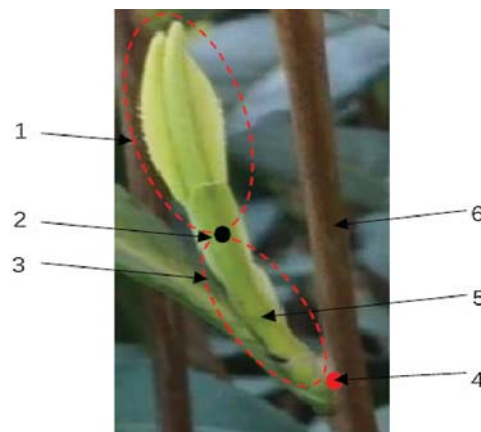

Figure 4: Picking point calculation model. 1. Tea sprout; 2. Lowest point of contour; 3. Ideal area for picking; 4. Corner point; 5. Petiole; 6. Branches

4.1 Feature Extraction

Fig. 5a shows the HSV color space of the ROI, from which the characteristics of the sprouts and their growth points are extracted, as follows.

(1) The H, S, and V channels are separated from the ROI of the HSV space. The upper and lower limits of the pixel values of the H, S, and V channels are set. The area where the sprouts

and branches are located is selected, and a *mask* as large as the original image is set as

$$mask = \begin{cases} 1, & min \leq src \leq max \\ 0, & src \leq min \ or \ max \leq src \end{cases}, \quad (3)$$

where *src*, *min*, and *max* are the pixel value and its lower and upper limits, respectively. The treatment results are shown in Figs. 5b–5d. In the HSV color space, the color difference of tea sprouts, old leaves, and branches is mainly manifested in their H channel values. After experimental comparison, the value ranges of the channels are set as $H = [80,150]$, $S = [35,250]$, and $V = [35,250]$.

(2) The sprouts and branches are extracted by the bitwise AND operation of ROI and *mask* in the RGB space. As shown in Fig. 5e, the results highlight the characteristics of tea sprouts and branches.
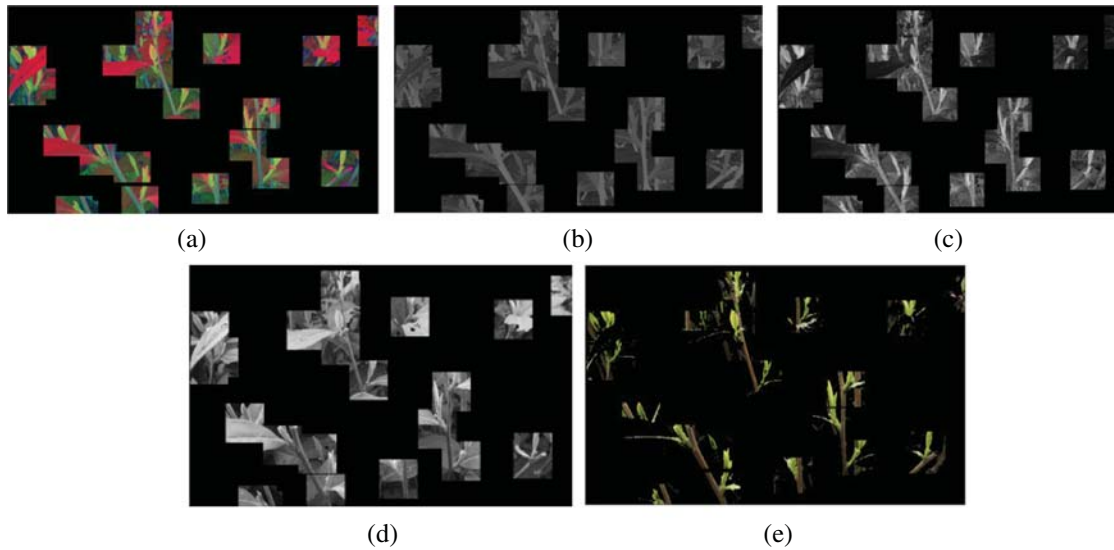

Figure 5: Extraction of sprout and branch features. a. HSV color space, b. H channel, c. S channel, d. V channel, e. Characteristics of sprouts and branches

4.2 Skeleton Refinement

The Otsu algorithm is used to binarize the image in Fig. 5e, and morphological manipulation corrosion is applied to remove small areas in the binarized image. Fig. 6 shows the result of binary and morphological processing.

The *Zhang* thinning algorithm is fast and can maintain the curve characteristics of the original image, with fewer burrs after thinning [14,15]. However, the thinning skeletons of sprouts and branches are incomplete, and all the curves cannot be kept as a single pixel. We apply an improved *Zhang* thinning algorithm [16]. A pixel at the boundary of a binary image is denoted as P_1, and eight neighboring pixels are denoted clockwise as P_2, P_3, …, P_8, P_9. P_2 is directly above P_1. The steps of the algorithm are as follows.

(1) Boundary points that meet the following conditions are marked simultaneously:

1) $2 \leq N(P_1) \leq 6$

2) $S(P_1) = 1$ or $B(P_1) \in \{5, 13, 20, 22, 52, 54, 65, 80, 133, 141\}$

3) $P_2 \times P_4 \times P_6 = 0$

4) $P_4 \times P_6 \times P_8 = 0$

(2) Boundary points that meet the following conditions are deleted simultaneously:

1) $2 \leq N(P_1) \leq 6$

2) $S(P_1) = 1$ or $B(P_1) \in \{5, 13, 20, 22, 52, 54, 65, 80, 133, 141\}$

3) $P_2 \times P_4 \times P_8 = 0$

4) $P_2 \times P_6 \times P_8 = 0$

where $N(P_1)$ is the number of nonzero neighbors of P_1, and $S(P_1)$ is the number of times the value changes from 0 to 1. When P_2, P_3, ..., P_8, P_9 is the order, $B(P_1)$ is the binary coded value of the P_1 eight-neighborhood point $B(P_1) = \sum_{n=2}^{9} (P_n \times 2^{n-2})$.

Iteration continues until all points meet the above conditions. The tea images' skeleton refinement results are shown in Fig. 7. The original tea branches and sprouts' growth features are retained, and a single-pixel skeleton is generated.
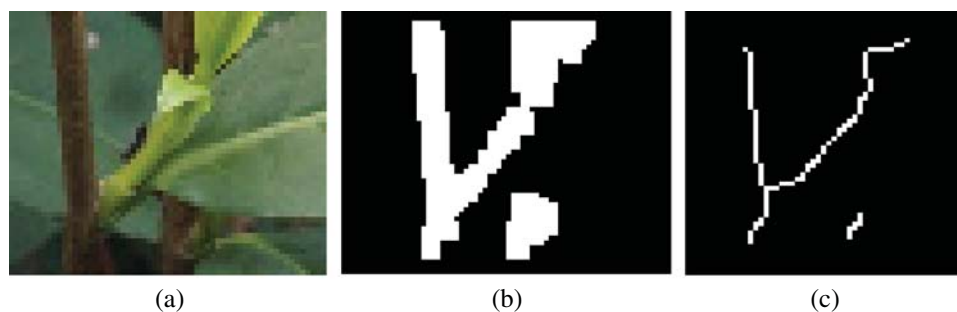

Figure 6: Secondary segmentation result

(a)   (b)   (c)

Figure 7: Skeleton thinning process and results. a. Original image b. Binarization c. Skeleton refinement

4.3 Corner Extraction of Skeleton

After refining, the bifurcation points of sprouts and branches must be determined as corner points. There are many corner detection methods, such as *Harris* corner detection algorithm and *Shi-Tomasi* corner detection [17–22]. The latter is used in this study.

Suppose the pixel coordinates of a point in the window are (x, y), the amount of movement is $(\Delta x, \Delta y)$, and the gray level is I. Then the gray level change is obtained as

$$E(\Delta x, \Delta y) = \sum_{x,y} \omega(x, y)[I(\Delta x + x, \Delta y + y) - I(x, y)]^2, \tag{4}$$

where the window function $\omega(x, y)$ is expressed by the Gaussian function as

$$\omega(x, y) = \exp\left(-\frac{x^2 + y^2}{2\sigma^2}\right). \tag{5}$$

The Taylor formula (4) is expanded, and the higher-order terms are omitted:

$$E(\Delta x, \Delta y) \cong [\Delta x \quad \Delta y] M [\Delta x \quad \Delta y]^T, \tag{6}$$

where

$$M = \exp\left(-\frac{x^2 + y^2}{2\sigma^2}\right) \otimes \begin{bmatrix} I_x^2 & I_x I_y \\ I_x I_y & I_y^2 \end{bmatrix}, \tag{7}$$

where I_x and I_y are the gradient values of the image gray in the x and y directions, respectively,

$$\begin{cases} I_x = \dfrac{\partial I}{\partial x} \\ I_y = \dfrac{\partial I}{\partial y} \end{cases}. \tag{8}$$

The corner response function is defined as

$$R = min(\lambda_1, \quad \lambda_2), \tag{9}$$

where λ_1 and λ_2 are the two eigenvalues of the matrix M.

When R exceeds the threshold T_0 and is a local maximum in its neighborhood, the point is a *Shi-Tomasi* characteristic corner point, and its coordinates (x', y') are output.

Fig. 8 shows the results of corner detection using the *Harris* and *Shi-Tomasi* algorithms, respectively. *Harris* is easily affected by the environment, and the number of detected wrong corner points (yellow dots in Fig. 8a) is high. *Shi-Tomasi* detects only one of the best points (the red dot in Fig. 8b); it is not easily affected by the environment, and it has a stronger adaptive ability. This method can avoid clustering. *Shi-Tomasi* is more suitable for complex and changeable tea sprout picking situations.
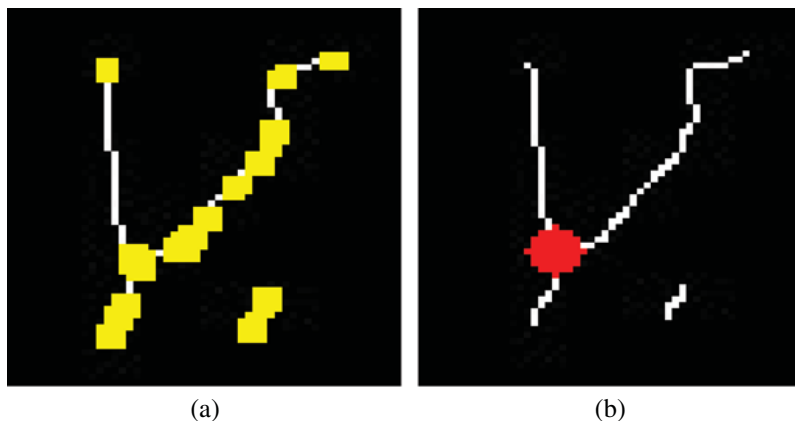
(a) (b)

Figure 8: Corner detection. a. Harris, b. Shi-Tomasi

4.4 Calculation of Picking Point

The lowest and corner points of the tea branches and sprouts' contours are fitted to a straight-line segment, and the center point is taken as the picking point, with horizontal and vertical coordinates expressed as

$$\begin{cases} u = \dfrac{x_0 + x'}{2} \\ v = \dfrac{y_0 + y'}{2} \end{cases}, \tag{10}$$

respectively.

5 Experimental Results and Analysis

5.1 Experimental Process

Tea samples were collected from the Shengzhou tea plantation base on March 11, 2020. We used an *FLIR BFS-U3-16S2C* industrial color area scan camera with a shooting angle of 45° from horizontal orientation. There were 60 groups of samples, and each group was run three times. The original image size was 1670 × 3000. The experimental process was conducted in the Python-OpenCV 4.1.1.26 algorithm environment on a BIS-6670 industrial computer (North China). The experimental results of the marked partial picking points are shown in Fig. 9, where *a–d* show partially marked successful picking points, and *e–h* are partially marked picking points that failed. The black points in the figure represent the lowest point of the initial segmentation contour, red dots indicate marked picking points, and blue dots are detected corners.

5.2 Analysis of Experimental Results

For tea sprouts with growth points hidden by branches and leaves, the red dot lies between the black and blue dots, and is in the ideal area of the tea petiole. The tea sprout's picking point is marked successfully; otherwise, it is recorded as a mark failure. The statistics of the identification of 60 groups of samples are shown in Tabs. 1–3.

The tables show that 1,545 tea sprouts were effectively identified in 60 groups of tea samples. Among them, 503 corner points were hidden and failed to be marked by default. The other 1,042 corner points were not hidden. Among the unhidden points, 887 corner points were successfully

marked. The effective marking success rate (*ES*) and overall marking success rate (*RS*) are defined as

$$ES = S/N \times 100\%, \tag{11}$$

$$RS = S/T \times 100\%, \tag{12}$$

where S is the number of successfully marked sprouts, N is the number of unobstructed sprouts, and T is the total number of identified sprouts. The effective labeling success rate and overall labeling success rate of the 60 groups of samples are shown in Fig. 10.
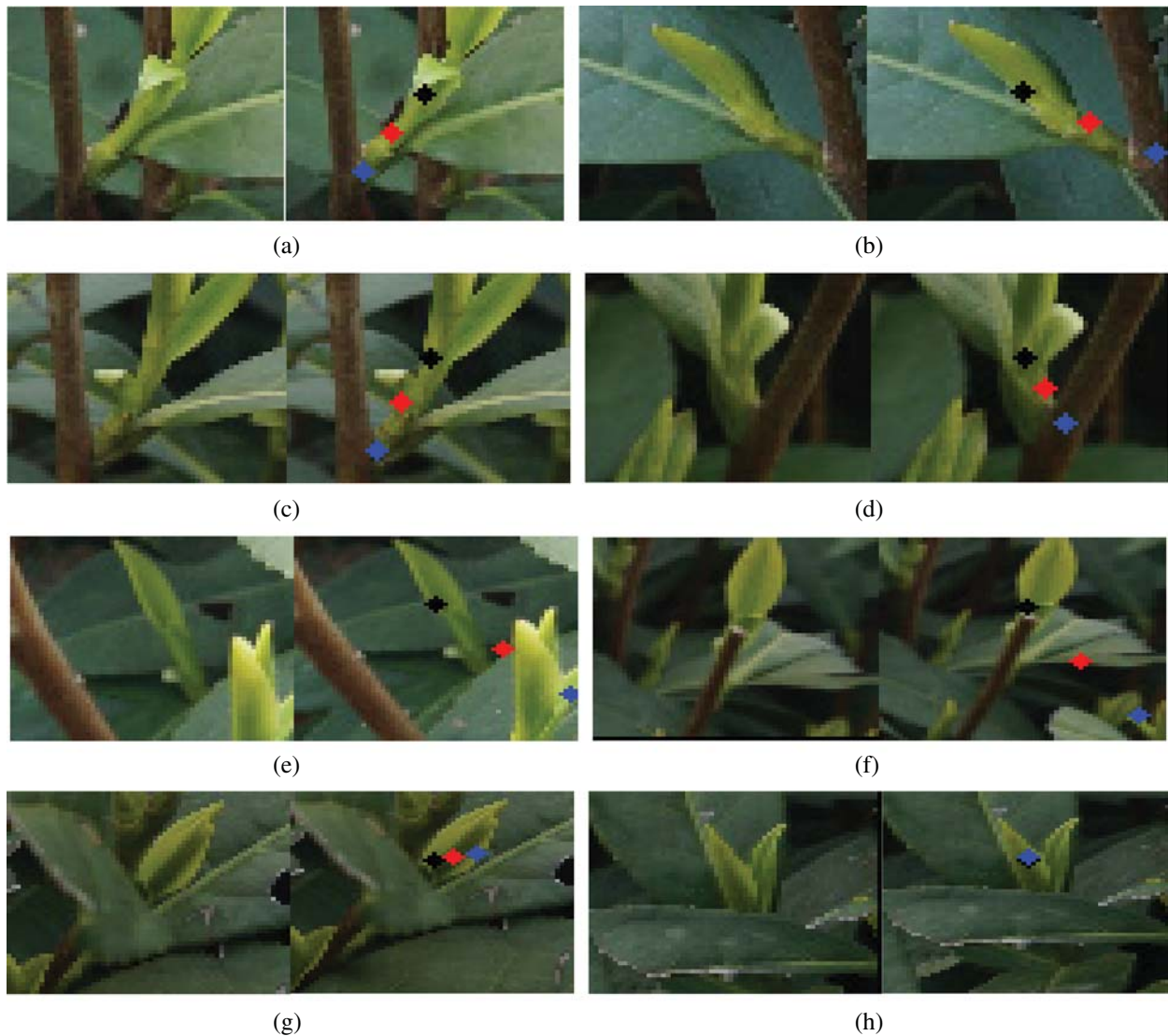

Figure 9: Marked results of picking points. a. Sprout 1, b. Sprout 2, c. Sprout 3, d. Sprout 4, e. Sprout 5, f. Sprout 6, g. Sprout 7, h. Sprout 8

Table 1: Data statistics 1 of test results

Samples	1	2	3	4	5	6	7	8	9	10	11	12	13	14	15	16	17	18	19	20
Total number	23	24	18	41	24	18	14	30	13	21	20	16	26	18	26	24	47	42	23	29
Obscured number	6	13	5	13	8	5	3	9	6	7	10	5	9	6	8	6	19	17	8	10
Un-occluded number	17	11	13	28	16	13	11	21	7	14	10	11	17	12	18	18	28	25	15	19
Number of successful markers	15	9	12	23	14	10	11	19	6	12	8	8	15	10	16	15	21	20	13	16

Table 2: Data statistics 2 of test results

Samples	21	22	23	24	25	26	27	28	29	30	31	32	33	34	35	36	37	38	39	40
Total number	41	30	39	28	17	25	14	25	19	32	37	41	18	27	21	18	29	33	23	16
Obscured number	17	13	15	8	2	4	3	3	4	8	11	11	4	8	5	4	9	12	7	4
Un-occluded number	24	17	24	20	15	21	11	22	15	24	26	30	14	19	16	14	20	21	16	12
Number of successful markers	20	15	21	17	12	19	10	19	14	19	22	24	12	16	14	13	17	17	13	11

Table 3: Data statistics 3 of test results

Samples	41	42	43	44	45	46	47	48	49	50	51	52	53	54	55	56	57	58	59	60
Total number	22	31	25	17	32	39	24	35	25	18	21	22	31	19	26	20	17	28	34	29
Obscured number	8	10	9	4	12	16	8	11	11	5	7	5	11	5	9	9	5	9	13	11
Un-occluded number	14	21	16	13	20	23	16	24	14	13	14	17	20	14	17	11	12	19	21	18
Number of successful markers	12	17	13	12	17	19	13	20	12	12	12	15	17	13	15	9	11	17	18	15

In the 60 groups of samples, the overall labeling success rate was 50%–65%, and the effective labeling success rate was 75%–90%. The average overall labeling success rate was 57.41%, and the average effective labeling success rate was 85.12%. The low success rate of overall labeling was mainly caused by a large proportion of tea sprouts hidden by old leaves, branches, or other objects, thereby making their identification impossible. Considering that the sprouts are picked and the camera moved during the picking process, the picking point of the hidden sprouts will be re-identified and positioned. The low success rate of effective labeling is mainly due to the complicated growth environment of tea sprouts and the interlacing of multiple branches in the ROI, which leads to deviations in corner monitoring and affects the accurate positioning of

picking points. The corner points of two or more tea sprouts are very close, and the petiole parts may overlap. This phenomenon leads to positioning errors of tea sprouts. Some sprouts bend greatly, thereby causing the positioning point to deviate from the petiole itself. The environmental light may be too strong or too dark while the tea images were obtained, thereby causing inaccurate segmentation of some tea sprouts. As a result, deviations occurred in the calculation of the coordinates of tea sprout picking points.
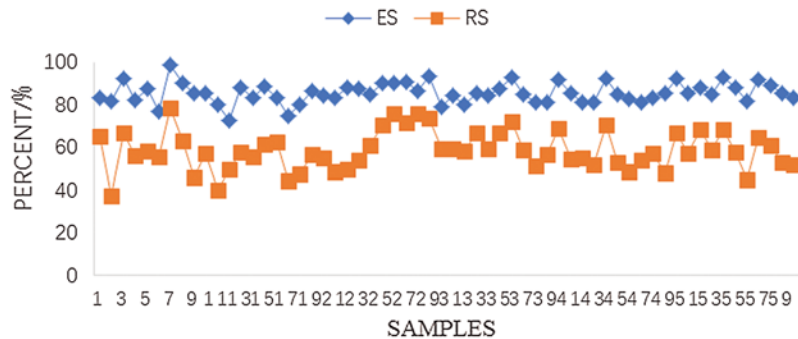

Figure 10: Effective marking success rate and overall marking success rate

We calculated the effective mark success rate of the picking points of sprouts, based on whether the picking point fell on the petiole. Sprouts whose marked picking point fell within a certain range around the petiole could also be obtained. Thus the actual effective picking rate obtained by this algorithm must have been higher than the labeling success rate of 85.12%.

6 Conclusion

We proposed a famous tea sprout automatic segmentation and positioning method based on the Otsu algorithm, improved Zhang thinning algorithm, and *Shi-Tomasi* algorithm. The Otsu algorithm was first used to segment the tea sprouts, and the ROI with the lowest point on its contour was set as the center. The characteristics of the sprouts and branches were extracted on the basis of the HSV space H channel, and the sprouts were segmented again with the Otsu algorithm. The sprouts' single-pixel feature was refined, and the *Shi-Tomasi* algorithm was used to detect the corner points of the sprouts on the branches. The line segment between the corner point and the lowest point was fitted, and the center point was taken as the picking point. The proposed algorithm effectively solved the problem of low accuracy of tea sprout automatic segmentation and positioning. The effectiveness of this algorithm was verified by using 60 sets of samples and by conducting marked experiments on 1,545 sprouts' picking points across these 60 sets. The reasons for the failed marking of picking points were analyzed from multiple aspects, thereby providing certain ideas for subsequent research on automatic picking of tea sprouts by robots. The proposed method had an effective marked success rate of 85.12% for the picking points of tea sprouts, thereby meeting the picking requirements of famous tea. This study provides a reference for the realization of mechanized automatic picking of famous tea.

Conflicts of Interest: The authors declare that they have no conflicts of interest to report regarding the present study.

References

[1] A. Renugambal and K. S. Bhuvaneswari, "Image segmentation of brain MR images using OTSU's based hybrid WCMFO algorithm," *Computers, Materials & Continua*, vol. 64, no. 2, pp. 681–700, 2020.

[2] B. T. Hu and J. W. Wang, "Deep learning for distinguishing computer generated images and natural images: A survey," *Journal of Information Hiding and Privacy Protection*, vol. 2, no. 2, pp. 37–47, 2020.

[3] D. Chaves, M. Trujillo, E. Garcia, J. Barraza, E. Lester *et al.,* "Automated inspection of char morphologies in colombian coals using image analysis," *Intelligent Automation & Soft Computing*, vol. 26, no. 3, pp. 397–405, 2020.

[4] E. M. Abdelkader, O. Moselhi, M. Marzouk and T. Zayed, "A multi-objective invasive weed optimization method for segmentation of distress images," *Intelligent Automation & Soft Computing*, vol. 26, no. 4, pp. 643–661, 2020.

[5] G. H. Yu, H. H. Fan, H. Y. Zhou, T. Wu and H. J. Zhu, "Vehicle target detection method based on improved SSD model," *Journal on Artificial Intelligence*, vol. 2, no. 3, pp. 125–135, 2020.

[6] X. F. Liang, C. Q. Jin, M. D. Ni and Y. W. Wang, "Acquisition and experiment on location information of picking point of tomato fruit clusters," *Transactions of the CSAE*, vol. 34, no. 16, pp. 163–169, 2018.

[7] C. H. Yang, Y. P. Liu and Y. Wang, "Research and experiment of recognition and location system for citrus picking robot in natural environment," *Transactions of the Chinese Society of Agricultural Engineering*, vol. 50, no. 12, pp. 14–22, 2019.

[8] L. T. Huang, B. Wang, T. Ni, H. Miao and Y. Li, "Research on robotic grasping system based on Kinect camera," *Transactions of the Chinese Society for Agricultural Machinery*, vol. 50, no. 1, pp. 390–399, 2019.

[9] J. T. Xiong, Z. L. He, L. Y. Tang, R. Lin and Z. Liu, "Visual localization of disturbed grape picking point in non-structural environment," *Transactions of the Chinese Society for Agricultural Machinery*, vol. 48, no. 4, pp. 29–33, 2017.

[10] D. D. Wang, Y. Xu, H. B. Song and D. J. He, "Localization method of picking point of apple target based on smoothing contour symmetry axis algorithm," *Transactions of the CSAE*, vol. 31, no. 5, pp. 167–174, 2015.

[11] L. F. Luo, X. J. Zou, J. T. Xiong, Y. Zhang, H. X. Peng *et al.,* "Automatic positioning for picking point of grape picking robot in natural environment," *Transactions of the CSAE*, vol. 31, no. 2, pp. 14–21, 2015.

[12] H. Zhang, Y. Chen, W. Wang and G. L. Zhang, "Positioning method for tea picking using active computer vision," *Transactions of the Chinese Society for Agricultural Machinery*, vol. 45, no. 9, pp. 61–65, 2014.

[13] W. Pei and X. L. Wang, "The two-dimension coordinates extraction of tea shoots picking based on image information," *Acta Agriculturae Zhejiangensis*, vol. 28, no. 3, pp. 522–527, 2016.

[14] M. W. Liu and L. X. Gu, "A fast LUT-based airway skeleton extraction algorithm for virtual bronchoscopy," *Journal of Harbin Institute of Technology*, vol. 49, no. 5, pp. 134–140, 2017.

[15] Q. L. Han, Y. Zhao, Y. D. Zhao, X. J. Pan, Y. Peng *et al.,* "Skeleton extracting algorithm for soil pore based on thinning method," *Transactions of the Chinese Society of Agricultural Engineering*, vol. 50, no. 9, pp. 229–234, 2019.

[16] S. M. Mu, H. Y. Du, P. Su, X. H. Zha and G. Y. Chen, "A new improved fast parallel thinning algorithm," *Mircoelectronics & Computer*, vol. 30, no. 1, pp. 53–55.60, 2013.

[17] Q. S. Liu, X. F. Xie and X. Z. Zhang, "Checkerboard corner detection algorithm for calibration of the focused plenoptic camera," *Acta Optica Sinica*, vol. 40, no. 14, pp. 1–14, 2020.

[18] Y. H. Li, Y. R. He and W. C. Zhang, "Image corner detection using recursively maximum point-to-chord distance," *Journal of Image and Graphics*, vol. 24, no. 7, pp. 1148–1159, 2019.

[19] W. C. Zhang, X. N. Kong and W. Song, "Review of image corner detection algorithms," *Acta Electronica Sinica*, vol. 43, no. 11, pp. 2315–2321, 2015.

[20] Y. X. Xing, D. Y. Zhang, J. H. Zhao, M. G. Sun and W. Y. Jia, "Robust fast corner detector based on filled circle and outer ring mask," *IET Image Processing*, vol. 10, no. 4, pp. 314–324, 2016.

[21] X. Y. Lin, C. Zhu, Y. P. Liu and Q. Zhang, "Geometric mesh corner detection using triangle principle," *Electronics Letters*, vol. 53, no. 20, pp. 1354–1356, 2017.

[22] Y. Li, J. Xu, R. Xia, Q. Huang, W. Xie *et al.,* "Extreme-constrained spatial spectral corner detector for image-level hyperspectral image classification," *Pattern Recognition Letters*, vol. 10, no. 9, pp. 110–119, 2018.